Journal of Rheology

RESEARCH ARTICLE | JANUARY 02 2025

A basic model for the nonlinear rheology of bijels

Herman Ching; Ali Mohraz

J. Rheol. 69, 45–54 (2025)
https://doi.org/10.1122/8.0000914

A basic model for the nonlinear rheology of bijels

Herman Ching and Ali Mohraz[a)]

Department of Chemical and Biomolecular Engineering, University of California, Irvine, California 92697-2580

(Received 8 September 2024; final revision received 3 December 2024; published 2 January 2025)

Abstract

We examine the rheology of bicontinuous interfacially jammed emulsion gels (bijels) beyond the limit of linear viscoelasticity and propose a simple model that connects bijel rheology to anticipated microstructural changes in the continuous particle-laden interface. The basic elements of our model are constructed from a linear stress relaxation experiment, which suggests glasslike rheology mediated by α (out-of-cage) and β (in-cage) particle dynamics along the interface in this limit. Extending to medium amplitude oscillatory shear experiments then reveals signatures of nonlinearity, which we rationalize as the combined effect of shear-induced dilation of the interface and its simultaneous recompaction by interfacial tension, as well as potential buckling along portions of the interface under compression. Informed by these observations, we present a double Maxwell model with sigmoidal nonlinearities introduced to account for how interfacial dilation and recompaction affect the intercage particle dynamics (α relaxation) along the interface and buckling. This simple model successfully captures the general features of nonlinear rheology in bijels, indicating that their linear-to-nonlinear transition is associated with loss of compaction along the dilated and buckling along the compacted regions of the interface. Our results shed initial light on the microstructural origins of nonlinear rheology in bijels and the reconfigurability afforded in these systems by the balance of glassy particle dynamics and interfacial recompaction under shear deformation. https://doi.org/10.1122/8.0000914

I. INTRODUCTION

Bicontinuous interfacially jammed emulsion gels, or bijels, are solid-stabilized emulsions uniquely characterized by two distinct fluid phases that are separated and mechanically stabilized by a continuous, sample-spanning particle-laden interface [1]. Bijels are typically formed by initiating spinodal decomposition in a dispersion of neutrally wetting nanoparticles [2–4]. During spinodal decomposition, the nanoparticles irreversibly adsorb to the continuous interface with adsorption energy $>10^3\, k_BT$ [5]. Reduction of the interfacial area due to interfacial tension brings the particles together until the surface coverage approaches the two-dimensional (2D) jamming limit for the type of particles used. Colloidal jamming along the continuous interface then kinetically halts the process and yields sufficient mechanical rigidity to sustain a self-standing, bicontinuous emulsion with a sample-spanning continuous interface with a predominance of zero mean, negative Gaussian, curvatures (saddle points) [6,7]. Importantly, the interfacial area per unit volume (or characteristic domain size) at the onset of jamming can be controlled via the volume fraction of nanoparticles (ϕ_{SNP}) [8–10]. The combination of these microstructural features makes bijels excellent candidates for template-based synthesis of functional materials with applications ranging from electrochemical devices [11–17] to catalysis and separations [18,19], regenerative biomaterials [20,21], and architected composites [22,23].

With several proof-of-concept applications as mentioned above already demonstrated, the next leap toward the development and implementation of bijel-derived technologies at scale requires a better fundamental understanding of bijel rheology [24,25]. This proposition is specifically motivated by the following two problems. First, one of the most prominent methods of bijel processing to date involves a monomer exchange step after bijel formation [26], which can lead to surface tension gradients along the jammed interface and a complete microstructural breakdown if the bijel cannot withstand the resulting Marangoni forces [27]. Second, a better understanding of bijel rheology, especially in the large strain limit, can lead to the development of cocontinuous composites with anisotropic transport and mechanical properties, a topic with significant technological potential that has remained largely unexplored. To address these concerns, Lee *et al.* conducted the first rheological study on water/2,6-lutidine (W/L) and nitromethane/ethylene glycol (NM/PG) bijels and concluded that greater interparticle attractions result in more mechanically robust bijels in the W/L system than their NM/PG counterparts [27]. Macmillan *et al.* later performed a rheological investigation combined with *in situ* confocal imaging on a particular class of bijels that are formed by direct mixing and provided evidence for two-step yielding and fluidization of the interface prior to shear-induced microstructural breakdown [28]. Bai *et al.* studied the dynamics and rheology of a nonpolar bijel and reported evidence of coarsening and particle rearrangements along the interface over long periods [30]. A review article by Thijssen and Vermant has provided important insights into the connection between interfacial rheology and stability of bijels [29]. Finally, in a recent study focused on the nature

[a)]Author to whom correspondence should be addressed; electronic mail: mohraz@uci.edu

of interparticle interactions in bijels, we demonstrated that the viscoelasticity of bijels made with 1,4-butanediol (BD), propylene carbonate (PC), and neutrally wetting silica nanoparticles (SNPs) can be attributed to interfacial jamming alone, and attractive interparticle interactions are not necessary for achieving mechanical stability in these systems, which do not form monogels [30,31]. In that work, the linear viscoelasticity of bijels was aptly described by an early adaption of the Mode Coupling theory first derived to model colloidal glasses, with signatures of α- and β-like relaxation mechanisms at long and short timescales [32]. These observations depicted bijels as 2D colloidal glasses wrapped in 3D, with glasslike viscoelasticity resulting from colloidal jamming along the continuous interface. This picture then raises the following intriguing question: if bijel viscoelasticity purely arises from interfacial jamming, how would the particle dynamics and rheology change in response to shear deformation in the intermediate strain regime? Bijels offer a unique manifestation of this problem since shear deformation can result in a net increase in the interfacial area, effectively unjamming the weaving 2D colloidal glass while interfacial tension continuously recompresses the interface toward its jamming limit [33,34]. In addition, portions of the sample-spanning jammed interface colinear with the rotational component of shear deformation can undergo local buckling at intermediate strains. Therefore, the rheology of bijels, especially at intermediate strain amplitudes, is likely governed by a rich rate-dependent competition between deformation-induced unjamming and recompression by interfacial tension, as well as potential buckling along a sample-spanning jammed interface.

To provide a general framework for investigating these questions, here we present a simple model for bijel rheology both within and beyond the linear viscoelasticity limit. The central concepts underlying our model are how the particle dynamics may be impacted by shear deformation, as well as how large deformations may lead to loss of elasticity and buckling in bijels. We first construct the model's basic elements from a stress relaxation experiment [35]. Nonlinear effects are then incorporated based on the anticipated dependence of particle dynamics on interfacial coverage and its relation to the rate and magnitude of shear deformation, as well as loss of elasticity due to unjamming of the particles, and potential buckling along the interface. We then test the ability of our simple model to capture the transition from linear-to-nonlinear viscoelasticity in bijels by comparing its predictions to experimental results in the context of Lissajous curves and frequency sweep measurements at intermediate strain amplitudes. We demonstrate that a simple double Maxwell representation of the system, based on the widely separated timescales for α- and β-relaxation modes and appropriate nonlinear effects to account for faster intracage dynamics and smaller elastic moduli at lower surface coverage, is able to represent the gross features of bijel rheology within and beyond the linear viscoelasticity limit. Overall, our findings provide a simple framework to understand bijel mechanics as well as affirm that glasslike particle dynamics play an essential role in the rheology of bijels and interfacial compaction is the predominant contributor to their viscoelasticity and mechanical stability. Furthermore, the onset of nonlinearity appears to originate from the deformation-induced local dilation and fluidization along the continuous interface as well as potential local buckling along its compressed regions.

II. MATERIALS AND METHODS

A. Materials

All materials were used as received. BD (99%), PC (99.7%), fluorescein isothiocyanate isomer I (FITC, ≥90%), and tetraethyl orthosilicate (≥99.0%) were purchased from Sigma Aldrich. (3-aminopropyl) triethoxysilane (APTES, ≥98%) was purchased from TCI America. HPLC grade water was purchased from Fisher Chemical. Strong ammonia hydroxide solution (27%–30%) was purchased from VWR. Anhydrous ethanol (200 proof) was purchased from Rossville Gold Shield. Hexamethyldisilazane (HMDS, 98+%) was purchased from Alfa Aesar.

B. Silica nanoparticle synthesis

Monodispersed, fluorescently tagged SNPs were synthesized using a modified Stöber process and subsequently silanized to achieve neutral wetting properties with respect to BD and PC. In brief, 8.0 mg of FITC and 33.8 µl of APTES were mixed into 6.4 ml of anhydrous ethanol for 15 min to synthesize a silane-conjugated fluorescent dye. Then, 1 ml of the dye solution, 1 ml of water, 680 µl of tetraethyl orthosilicate, and 295 µl of strong ammonia solution were added to 8.8 g of anhydrous ethanol and allowed to react for 3 h under mild stirring at 4 °C. Next, 175 µl of HMDS was added to the reaction mixture and allowed to react for 18 h. In our experience, bijel formation is generally sensitive to even small variations in the surface chemistry of SNPs, and such variations are expected from batch to batch, depending on environmental conditions such as temperature and relative humidity. Therefore, neutral wetting conditions were assessed directly by confocal laser scanning microscopy (CLSM, Olympus Fluoview 3000) visualization of successful bijel formation (see Sec. II C). The resulting particles were recovered via centrifugation and washed by resuspension in anhydrous ethanol. After three washes, the particles were dried in a 110 °C vacuum oven for 1 h. The particle size distribution (radius, a = 160 nm and coefficient of variance, CV = 6.7%) was determined using scanning electron microscopy (SEM, FEI Magellan 400 XHR). A representative SEM micrograph of the particles is shown in Fig. S1 in the supplementary material.

C. BD/PC bijel formation

A nonvolatile fluid mixture comprising BD and PC was chosen to prepare bijels for extensive rheological characterization. First, an ultrasonic horn (Sonifier 250, Branson Ultrasonics) was used to disperse SNPs in a critical mixture of BD and PC (56.0 vol. % PC) at a particle volume fraction (ϕ_{SNP}) of 1.5%. The vigorous sonification also heated the mixture to above its upper critical solution temperature of 30.3 °C [30]. To assess the wettability of SNPs with respect

to BD and PC, a small aliquot of this heated and sonicated suspension was transferred to a preheated glass cuvette (400 μm ID, VitroCom), and the cuvette was placed in contact with a room temperature heat sink (~22 °C) to initiate phase separation of the binary fluid mixture. SNPs with too much HMDS or too little HMDS coupled to the particle surface would produce discrete droplets, while neutrally wetting SNPs produced bicontinuous structures [33]. In this study, the criteria for successful bijel formation are the presence of bicontinuous fluid domains and relative uniformity in the domain sizes, assessed through CLSM imaging. A confocal laser scanning micrograph of a bijel with these characteristics is shown in Fig. 1.

D. Bijel rheology

The rheology of the BD/PC bijels was characterized using a stress-controlled rheometer (DHR-3, TA Instruments, New Castle, DE) equipped with a cone-and-plate geometry (2°, 40 mm diameter, sandblasted, 60 μm truncation gap) and a temperature-controlled bottom plate. Bijels were formed on the rheometer using SNPs that had been tested by CLSM for successful bijel formation. To form the bijels, the warm dispersion (of SNPs suspended in the binary BD/PC fluid mixture) was transferred directly to the preheated (36 °C) rheometer stage and presheared at $30\ s^{-1}$ for 20 s. Then, a rapid quench (approx. −0.35 °C/s) to a final temperature of 21 °C was applied to initiate bijel formation. Meanwhile, a 2 h long oscillatory shear test (strain amplitude $\gamma_0 = 1.0 \times 10^{-1}\%$, frequency $\omega = 6.3 \times 10^{-1}$ rad/s, and sampled at three cycles per data point) was applied to monitor the bijel formation process. Based on the results (see Fig. S2 in the supplementary material), and also as established in our previous study, this waiting period was long enough for the viscoelastic moduli to reach their plateau values, presumably via slow particle rearrangements along the interface to approach the maximum close packing limit [30,36]. After bijel formation, the rheometer stage was held at a constant 21 °C for all subsequent experiments.

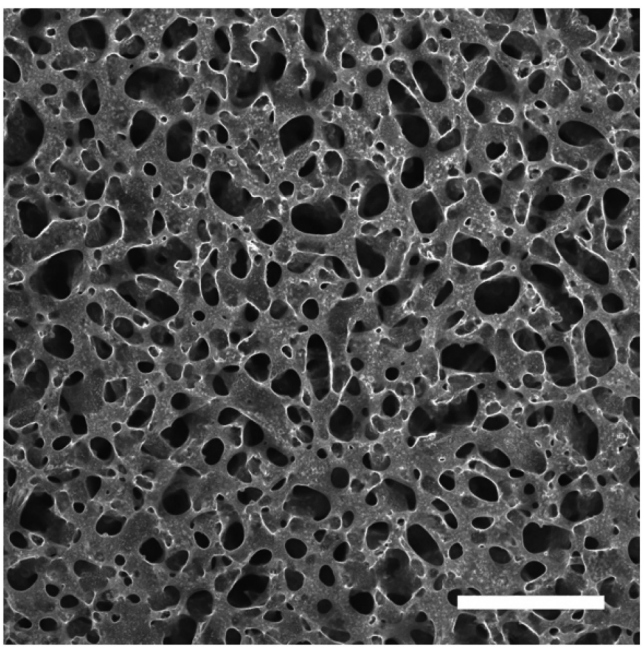

FIG. 1. Confocal laser scanning micrograph of a BD/PC bijel prepared with $\phi_{SNP} = 1.5 \times 10^{-2}$. The fluid interfaces are laden with a jammed monolayer of fluorescently tagged SNPs. Scale bar = 200 μm.

To measure the stress relaxation spectrum, a $\gamma = 0.5\%$ step strain (rise time 0.01 s) was applied to the bijels after the 2 h wait period, and stress was monitored for 24 h at the fastest accessible sampling rate on the rheometer. To gather transient stress and strain waveforms, small amplitude oscillatory shear (SAOS, $\gamma_0 = 0.1\%$) was first applied to a bijel at four fixed frequencies ($\omega = 1.3 \times 10^{-1}$, $6.3\times\ 10^{-1}$, 0.63, and 6.3 rad/s). Then, on the same bijel, medium amplitude oscillatory shear (MAOS) was applied for the same frequencies at $\gamma_0 = 1\%$, then 5%, and last, 10%. In these SAOS-MAOS tests, three cycles at $\omega = 1.3 \times 10^{-1}$ and 6.3×10^{-1} rad/s and six cycles at $\omega = 0.63$ and 6.3 rad/s were applied with a minimum sampling rate of 488 pt/cycles. The last oscillation cycle at each test was isolated to obtain the near-steady-state stress and strain information. This sequence of oscillatory shear from low to medium amplitudes minimizes the chances of shear-induced degradation of the notably weak bijel microstructure. SAOS-MAOS frequency sweeps were conducted in a similar sequence. In each experiment, a frequency sweep ($\omega = 6.3 \times 10^{-3} - 3.1 \times 10^{2}$ rad/s) was applied to a freshly prepared bijel at $\gamma_0 = 0.1\%$. Then, the same frequency sweep was repeated on the sample at $\gamma_0 = 1\%$, 5%, and 10%. To manage the duration of the experiments, each frequency sweep was divided into a low range ($\omega = 6.3 \times 10^{-3} - 6.3$ rad/s) with three cycles/pt and a high range ($\omega = 6.3 \times 10^{-1} - 3.1 \times 10^{2}$ rad/s) with 50 cycles/pt, which were conducted sequentially. No significant variations were observed in the overlap region of these experiments. A typical frequency sweep would take approximately 9 h to complete under our testing conditions. To assess the integrity of our samples after one of these lengthy tests, we performed an experiment in which a bijel at $\phi_{SNP} = 7.5 \times 10^{-3}$ was subjected to two sequential frequency sweeps in opposite directions (low-to-high frequency first, followed by high-to-low). The results, shown in Fig. S3 in the supplementary material, show a complete overlap of the two sequential tests, confirming that the rheological signatures of our samples did not change in timescales relevant to our tests. Nevertheless, we opted to limit the number of lengthy oscillation cycles to minimize potential minor changes to particle contact angles with prolonged exposure to the binary liquid mixture, which our model does not account for.

III. MODEL DEVELOPMENT, RESULTS, AND DISCUSSION

Recently, we presented evidence of distinct short- and long-time dynamics in bijels that we analogized to the in-cage (β-relaxation) and out-of-cage (α-relaxation) dynamics found in colloidal glasses [30]. Similar behaviors where the system's relaxation dynamics are primarily dominated by two widely separated timescales have been reported for various other disordered materials such as colloidal glasses and gels [37,38], concentrated emulsions [39,40], melts of

hyperstar polymers [41,42], as well as grafted nanoparticle melts [43]. In bijels, shear deformation can also lead to local compression, extension, and bending at different points on the continuous interface, leading to rheological phenomena not seen in their 3D colloidal glass analogs. Inspired by evidence for at least two widely separated relaxation timescales in bijels, here we propose a simple viscoelastic model for bijels comprising two Maxwell paths in parallel as a starting point. In a Maxwell system, the distribution of recoverable (γ_e) and unrecoverable (γ_v) strain (with total strain $\gamma = \gamma_e + \gamma_v$) can be determined by the overall shear rate ($\dot{\gamma}$) and the characteristic relaxation time $\tau = \eta/G$, where η is the dashpot viscosity and G is the spring constant. In our model, one spring and dashpot set ($n = 1$, where n is a counter to differentiate the two viscoelastic pathways) represents the short time (high frequency) response corresponding to the fast, in-cage motions of particles trapped by their neighbors, while the other set ($n = 2$) describes the long time (low frequency) behavior primarily comprising out-of-cage particle exchanges along the jammed interface ($\tau_2 >> \tau_1$). Together, the total stress is defined as $\sigma = \sigma_1 + \sigma_2$, while each Maxwell path is governed by the constitutive equation

$$\dot{\sigma}_n + \frac{G_n}{\eta_n}\sigma_n = G_n\dot{\gamma}, \tag{1}$$

where the dot notation represents a time derivative. Note that a continuous relaxation spectrum or a statistical model such as the Mode Coupling theory would more accurately depict the Brownian dynamics of colloids sequestered at the interface. However, here our goal is to provide a mathematically simple macroscopic description for modeling the response of bijels to medium strain deformations and their transition to nonlinear viscoelasticity.

As stated earlier, shear deformation can bring about interfacial dilation, which would reduce the overall 2D packing of particles along the interface and render their dynamics less constrained. Given that bijels attain their mechanical rigidity from the jammed particle monolayer, a reduction in surface coverage would result in a loss of elasticity, similar, in principle, to diluting a 3D colloidal glass [44]. However, unlike 3D colloidal glasses, there is a competing effect where the particle-laden interface is continuously driven back toward its fully packed limit by interfacial tension. Independently, local compaction of the continuous interface along the rotational axis of shear deformation can lead to buckling, further contributing to loss of elasticity. Based on these considerations, the central premise in our nonlinear model is how shear-induced interfacial dilation may affect the particle relaxation dynamics, as well as how shear deformation may lead to an overall loss of elasticity in the system. To account for these effects, we propose nonlinear G_2 and η_2 functions in our model, as schematically shown in Fig. 2.

Analogous modifications have been implemented previously by Kamani *et al.* and de Souza Mendes to describe the linear-to-nonlinear transition of structured yield stress fluids such as glasses and gels [45,46]. Kamani's treatment incorporated a Herschel–Bulkley representation of the dashpot

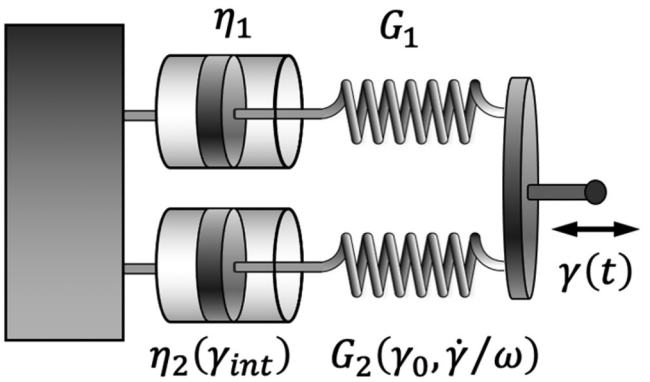

FIG. 2. Schematic illustration of the nonlinear double Maxwell viscoelastic model, with $n = 1$ (top row) corresponding to fast, in-cage particle dynamics, and $n = 2$ (bottom row) representing slow, cage relaxation along the interface. For this study, G_1 and η_1 are held constant, while G_2 and η_2 are defined as functions of the interfacial strain γ_{int}, strain amplitude γ_0, and the frequency-normalized shear rate $\dot{\gamma}/\omega$.

viscosity to model plastic deformation in yield stress fluids. Alternatively, de Souza Mendes proposed the use of a structural factor λ which influences the functions $G(\lambda)$ and $\eta(\lambda)$, to account for shear-induced microstructural changes in the system. As an example of a stepwise constitutive law, Dimitriou *et al.* defined a critical stress at which the material properties switched from linear to nonlinear to specify the onset of plasticity [47]. In bijels, particle mobility is tied to the excess interfacial area that is created by shear deformation. Therefore, we introduce a shear rate-dependent interfacial strain γ_{int} to relate particle dynamics to the applied deformation. The evolution of γ_{int} is governed by the ordinary differential equation

$$\frac{d\gamma_{\text{int}}}{dt} = \dot{\gamma} - R_f\gamma_{\text{int}}, \tag{2}$$

where R_f (=2.5 s^{-1} by data fitting—see below) represents the restorative character of the continuous interface due to interfacial tension. Physically, this equation tracks the excess interfacial area (represented as a dimensionless strain) created through the competition between affine deformation and tension-induced retraction. For oscillatory shear $\gamma(t) = \gamma_0\sin(\omega t)$, the above equation has the solution

$$\gamma_{\text{int}} = \frac{-\gamma_0 R_f\omega}{R_f^2 + \omega^2}e^{-R_f t} + \frac{\gamma_0\omega(R_f\cos(\omega t) + \omega\sin(\omega t))}{R_f^2 + \omega^2}. \tag{3}$$

We postulate that as γ_{int} increases, excess interfacial area loosens the particle network and increases particle mobility. As such, the α relaxation time scale, τ_2, shortens. To model this transition, we define $\eta_2(\gamma_{\text{int}})$ with a sigmoid function that weakens at large γ_{int}, defined by

$$\eta_2(\gamma_{\text{int}}) = \eta_0 10^{\left(\frac{c_1}{1+c_2|\gamma_{\text{int}}|^{c_3}} - c_1\right)}. \tag{4}$$

Here, $\eta_0 = 4 \times 10^4$ Pa s, $c_1 = 5.4$, $c_2 = 11.75$, and $c_3 = 0.3$ are fitting parameters defining the sigmoid function's height,

decay rate, and inflection point, which are obtained by nonlinear fitting to experimental data and subsequent manual inspection of the results. The resulting sigmoid function describing $\eta_2(\gamma_{\text{int}})$ is shown in Fig. S4(a) in the supplementary material.

We next incorporate into our model other nonlinear phenomena such as a general loss of elasticity at intermediate strains and potential buckling along the particle-laden interface. We anticipate buckling to depend on the applied strain with its propensity being highest during the high-rate portions of each oscillation cycle where the deformation rate overcomes the particles' ability to rearrange along the compressed regions. To incorporate these physics into our simple model, we propose a nonlinear G_2 function with sigmoid-based softening effects as shown below:

$$G_2\left(\gamma_0, \frac{\dot{\gamma}}{\omega}\right) = G_0 * G_a(\gamma_0) * G_r\left(\frac{\dot{\gamma}}{\omega}\right) = G_0 10^{\left(\frac{c_4}{1+c_5\gamma_0^{c_6}} - c_4\right)} 10^{\left(\frac{c_7}{1+c_8(\dot{\gamma}/\omega)^{c_9}} - c_7\right)}. \quad (5)$$

Here, $G_0 = 15$ Pa, $c_4 = 65$, $c_5 = 0.04$, $c_6 = 0.35$, $c_7 = 29.9$, $c_8 = 0.126$, $c_9 = 1.15$ obtained by fitting to experimental data and subsequent manual inspection of the results. The function $G_a(\gamma_0)$ represents the overall loss of elasticity at intermediate strains [30], and $G_r(\dot{\gamma}/\omega)$ captures the softening effects localized to high shear-rate portions of the oscillation cycle. The resulting sigmoid functions describing $G_a(\gamma_0)$ and $G_r(\dot{\gamma}/\omega)$ are shown in Figs. S4(b) and S4(c) in the supplementary material, respectively. Combining the nonlinear η_2 and G_2 functions into the Maxwell model results in the following constitutive equation:

$$\dot{\sigma}_2 = \frac{\dot{G}_2\left(\gamma_0, \frac{\dot{\gamma}}{\omega}\right)}{G_2\left(\gamma_0, \frac{\dot{\gamma}}{\omega}\right)}\sigma_2 + G_2\left(\gamma_0, \frac{\dot{\gamma}}{\omega}\right)\left(\dot{\gamma} - \frac{\sigma}{\eta_2(\gamma_{\text{int}})}\right). \quad (6)$$

The above ordinary differential equation was solved numerically using Wolfram Mathematica software. Note that our model incorporates nonlinear effects only in the $n = 2$ path of the double Maxwell model. This choice is motivated by two arguments. First, we postulate that shear-induced interfacial dilation will primarily impact the α-relaxation dynamics in the jammed particle layer, which are associated with cooperative out-of-cage rearrangements. Second, each form of nonlinearity introduced adds complexity and adjusting parameters to the analysis, both of which we are hoping to minimize in our basic model. Therefore, less influential shear-induced phenomena such as potential changes to the fast, in-cage dynamics of the particles, while acknowledged, are not accounted for in our basic model. To test the validity of our model, we next test its predictions against oscillatory experiments in the low- and intermediate-strain regimes.

As a first test, in Fig. 3, we present examples of the stress response of bijels to small and medium strain oscillatory shear ($\gamma_0 = 0.1\%$ and 10%, respectively) at low frequency ($\omega = 0.009$ rad/s), where our model's predictions are compared to experimental data. The experimental stress profile appears to be sinusoidal at $\gamma_0 = 0.1\%$, indicating a linear viscoelastic response [Fig. 3(a)]. Medium strain deformation brings about distortions from a sinusoidal pattern, where the stress response has a backward-tilted shape in its half-cycle [Fig. 3(b)] [48]. These nonsinusoidal fingerprints contain important information about yielding, which is not captured by the calculation of storage (G') and loss (G'') moduli from the data. The model produces a linear (sinusoidal) viscoelastic response at a small strain amplitude that mirrors the experimental results [Fig. 3(c)] and also successfully captures the general nonlinear features seen at medium strain amplitude. Specifically, it predicts the rapid drop in stress upon strain reversal at $|\gamma| = \gamma_0$ and the increased plasticity near high $\dot{\gamma}$, which, when combined, produce a backward-tilted stress response at $\gamma_0 = 10\%$ and $\omega = 0.009$ rad/s [Fig. 3(d)].

We next extend our analysis to a wider range of strain amplitudes and frequencies in Fig. 4, where the stress response to oscillatory strain cycles is represented as normalized Lissajous curves (σ/σ_0 vs. γ/γ_0) at four different frequencies and four different strain amplitudes, for both experiments and model predictions. We focus our analysis on variations in the shapes of the Lissajous curves in transition from the linear to the nonlinear regime, where several key signatures are observed in the experimental results. First, as the strain amplitude is increased, the samples generally exhibit more dissipative behavior, marked by an increase in the area enclosed within each cycle. Second, nonlinearities in the stress-strain cycles begin to appear as deviations from symmetric elliptical loops. Third, in the low frequency and high strain limits ($\gamma_0 = 5\%$ and 10%, $\omega = 0.009$ rad/s), the Lissajous curves appear as parallelogramlike shapes, signifying a region of constant elastic modulus followed by precipitous drops in stress when the oscillation changes direction at maximum/minimum strain. We interpret these nonlinear signatures in the context of changes in the mobility of particles under large strain deformation, as well as potential local buckling where the interface undergoes compression. At sufficiently low frequencies, shear-induced interfacial dilation occurs at a rate slower than surface tension-driven contraction, and the interface remains densely covered throughout the oscillation cycle. It is also plausible to expect little to no interfacial buckling at low frequencies since particle rearrangements can mitigate compressional stresses along the interface. We envision that the Lissajous curves at $\omega = 0.009$ rad/s represent this limit. In this regime, as the shear rate slows down to zero (or $|\gamma| \to \gamma_0$) corresponding to the top right and bottom left corners of each Lissajous curve, the interface is fully jammed. Strain reversal at this point results in rapid stress relief, which explains the nearly vertical profiles at the $|\gamma| = \gamma_0$ corners (for example, see the curves at $\omega = 0.009$ rad/s; $\gamma_0 = 5\%$ and 10%). By contrast, at sufficiently high frequencies the interface is both stretched faster than it can recoil and compressed faster than particle rearrangements can accommodate, resulting in locally reduced particle coverage and enhanced particle mobility along the stretched regions, as well as a higher propensity for buckling along the compressed areas. Both effects lead to increased

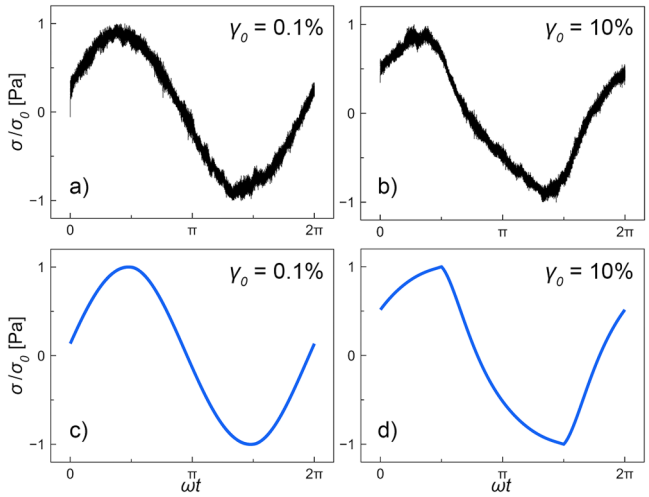

FIG. 3. Normalized stress response (σ/σ_0) of bijels under 0.1% (a) and 10% (b) oscillatory strain plotted as a function of ωt ($\omega = 0.009$ rad/s). The corresponding normalized stress responses simulated from the nonlinear double Maxwell model are shown in panels (c) and (d).

dissipative behavior especially during the high-rate portions of the oscillation cycle, producing the dilated elliptical shapes seen at $\omega = 0.6$ and 6 rad/s. The curve at $\omega = 0.06$ rad/s and $\gamma_0 = 10$ then represents an intermediate case between these low and high frequency regimes, and a Lissajous curve that combines their respective nonlinear signatures. Comparing the results between the experiments and model predictions at low strain amplitude (bottom row in Fig. 4), the model reproduces the increased viscous behavior (larger enclosed areas within the loops) at low and high frequencies seen in experiments, which correspond to the two time scales τ_2 and τ_1 associated with α and β relaxation of the jammed particle layer, respectively. Across the tested frequencies, the model also correctly predicts enhanced viscous behavior at larger γ_0, i.e., the normalized Lissajous curves become increasingly circular with larger enclosed areas at higher strain amplitudes. Finally, in the medium strain amplitude and low frequency regime, the model replicates the rapid drop in stress near the maximum/minimum strain, followed by a region of nearly constant elastic modulus. Overall, our mathematical formulation of the strain softening effects based on shear-induced dilation of the interface and enhanced particle mobility, loss of elasticity, and potential buckling demonstrates reasonable success in qualitatively capturing the transition from linear-to-nonlinear rheology in bijels.

To further test our model, in Fig. 5, we present experimental results and model predictions for small- to medium-strain oscillatory frequency sweeps, presented in the context of storage and loss moduli, G' and G''. We note that the definitions of G' and G'' are only formally valid within the linear viscoelasticity regime, and representation of the rheological

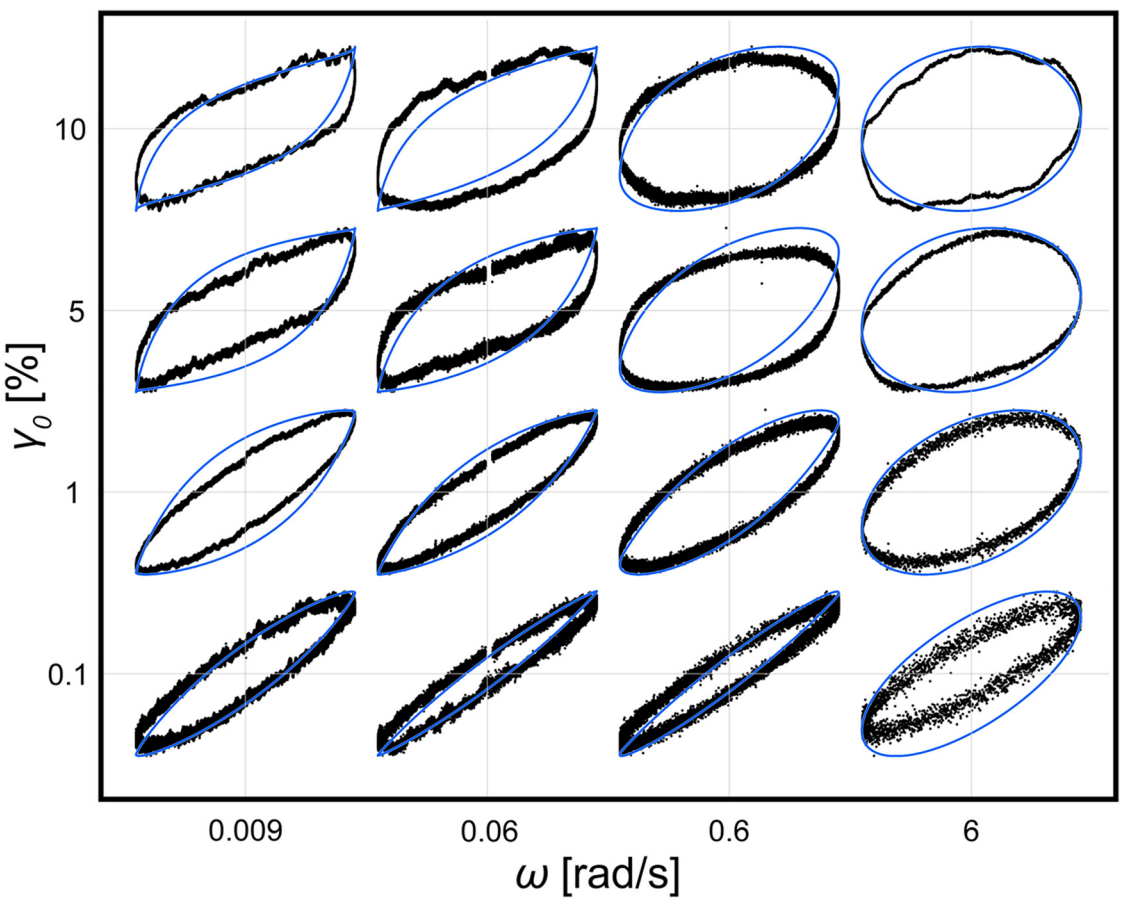

FIG. 4. Lissajous plots (stress vs strain) of bijels under SAOS and MAOS at different oscillation frequencies (ω). Each Lissajous plot was normalized to its stress amplitude (σ_0) and stain amplitude (γ_0). Experimental data points are plotted as circles, and model predictions are shown as solid lines. A 500 point (recorded at ~488 pt/s) running average was applied to the experimental results to smooth out the measurement noise.

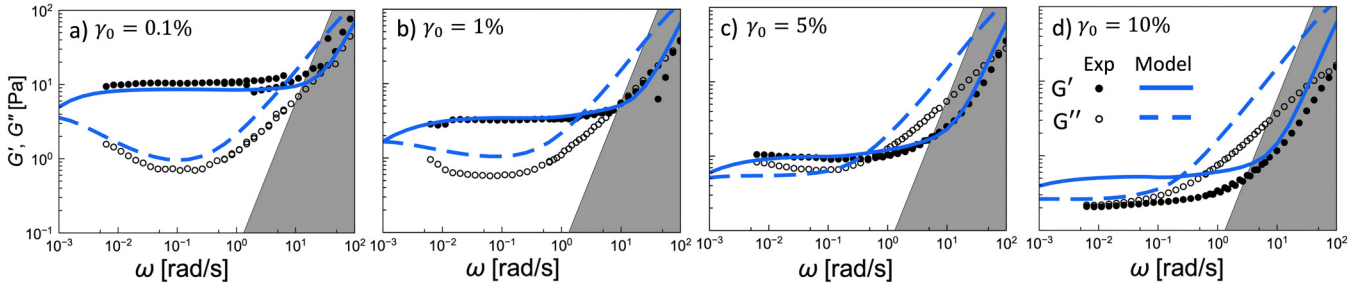

FIG. 5. Frequency sweeps of BD/PC bijels at small and medium strains, compared to predictions of the nonlinear double Maxwell model. The gray area in each plot represents the experimental range where the instrument inertia is significant and may potentially dominate the experimental results [35].

properties using these definitions disregards the detailed nonlinear components of the stress response and reports only its primary harmonic. Nonetheless, these representations capture overall changes in the magnitudes of viscoelastic moduli as well as the general timescales at play under medium strain deformation, which can prove insightful as complementary measures to the Lissajous plots presented in Fig. 4. In our previous documentation of bijel rheology [30], we attributed the minimum in G'' [also seen in Fig. 5(a)] to the competition between α and β dynamics. In addition, we previously reported the gradual disappearance of the minimum in G'' as γ_0 was increased beyond its linear limit [also seen in Figs. 5(b)–5(d)]), which was attributed to how shear-induced dilation of the interface enhances the dynamics of α-relaxation. To test the theory proposed in this paper, we compare experimental measurements of G' and G'' to our nonlinear double Maxwell model predictions. In the low strain limit [$\gamma_0 \leq 0.1\%$, Fig. 5(a)], our model predicts a nearly flat G' response and a minimum in G'' that mirror the experimental data. Upon increasing γ_0, the increased plasticity generated by the shear-induced weakening of G_2 and η_2 in the model results in an overall lowering of G' consistent with the experiments. Moreover, our model correctly predicts the flattening of the low-frequency G'' and the gradual disappearance of a minimum as γ_0 is increased beyond its linear limit. Remarkably, incorporating simple assumptions regarding the origin of nonlinearities in bijels, specifically the interplay between α and β dynamics, shear-induced dilation and recompaction of the interface, and potential buckling along the compressed segments of the interface into a simple double Maxwell model successfully predict the general features of the linear and nonlinear viscoelastic responses. The applicability of our model corroborates that the rheology of bijels is primarily governed by particle-induced stresses and, particularly, the disruption and simultaneous recovery of glassy colloidal dynamics along the jammed continuous interface. We will further elaborate on this issue below, before closing.

As another test of our model's predictions complementary to that shown in Fig. 5, we examined the relaxation dynamics of bijels in response to an initial step strain. An example of stress relaxation behavior in response to a $\gamma = 0.5\%$ step strain is plotted in Fig. 6, together with the predictions of our model. The sample exhibits an initial shear modulus of $G \sim 500$ Pa, which subsequently relaxes to a near stress-free state in two distinct steps with widely separated timescales, further corroborating the general picture that our model is based on. In such an experiment, interfacial dilation only occurs during the initial rise time. Further, local compressions caused by the sudden step strain can prompt particle jamming further into the glassy state akin to shear-induced jamming in 3D colloidal glasses [49] or result in buckling as discussed earlier. At short timescales, hindered particle motions within their respective cages can partially relax the accumulated stresses, but the overall system remains predominantly locked in a nonflowing state [50]. Over time, particle exchange between the cages eventually dissipates all local stresses throughout the interface [51]. The lack of a third, long-lasting plateau confirms that the deformation-induced stresses along the interface can be fully relaxed by slow α-relaxation, and the sample can be generally viewed as a viscoelastic liquid. Our basic model correctly captures the general behavior seen experimentally and provides a quantitative measure for the two timescales at play, with $\tau_1 = \eta_1/G_1 = 1.7 \times 10^{-3}$ s (β-relaxation timescale) and $\tau_2 = \eta_2/G_2 = 2.9 \times 10^{3}$ s (α-relaxation timescale in the absence of interfacial dilation).

To further investigate the dynamics of cage relaxation along the interface, we numerically determine how the α-relaxation timescale τ_2 varies throughout an oscillation cycle. In Fig. 7, we plot $\tau_2(\omega t)$ normalized by its maximum

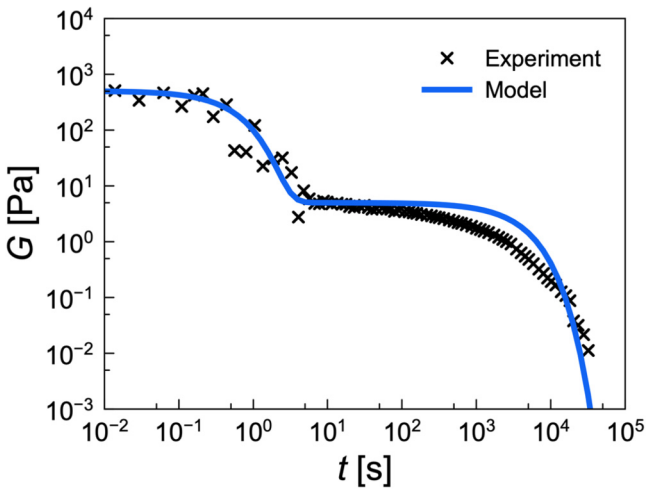

FIG. 6. Stress relaxation behavior of BD/PC bijels in response to a step strain at $\gamma = 0.5\%$ (rise time <0.01 s), where the stress response $\sigma(t)$ is plotted as the shear modulus $G(t) = \sigma(t)/\gamma$.

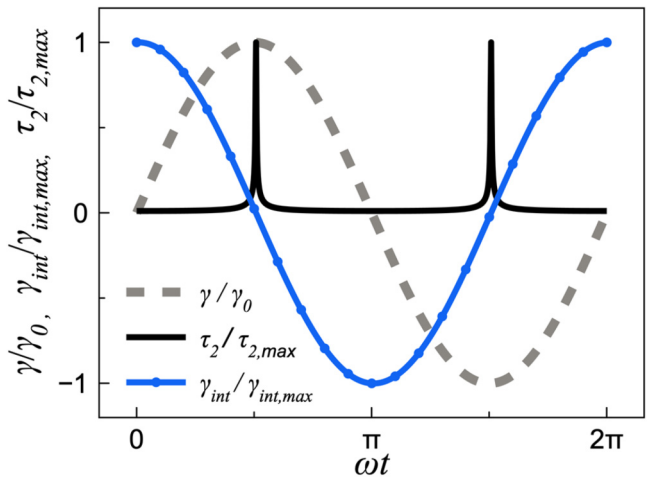

FIG. 7. α-relaxation timescale of bijels, τ_2, as predicted by the nonlinear double Maxwell model under MAOS ($\gamma_0 = 5\%$) during an oscillation cycle ($\omega = 0.06$ rad/s). To help interpret the results, the applied strain, γ, and the interfacial strain, γ_{int}, are also plotted. All three variables are normalized by their maximum value.

value alongside $\gamma(\omega t)$ and $\gamma_{int}(\omega t)$ during an oscillation cycle at intermediate strain amplitude ($\gamma_0 = 10\%$) and low frequency ($\omega = 0.009$ rad/s), where nonlinearities were fully apparent. The model predicts a dramatic peak in τ_2 when $|\gamma_{int}|$ drops to zero, and a precipitous drop in τ_2 once the interface is unjammed by dilation. This behavior aligns with our conjecture that excess interfacial area caused by shear deformation facilitates particle escape from cages, enhancing α-relaxation dynamics along the stretched portions of the interface.

Our adaptation of the nonlinear Maxwell model provides insights into the dynamics of particles under stress and their consequential nonlinear relaxation. However, the exact underlying physics of the rich nonlinear rheology of bijels must be further studied by more sophisticated statistical models with information regarding the ergodicity of the particle network [32]. The dynamics of particles along the interface are likely highly heterogeneous during shear deformation since extension, compression, shearing, and bending of the interface all dramatically impact local particle configurations in different ways. Such dynamical heterogeneities were grossly simplified in the adaptation of our simple spring and dashpot model. More direct mapping of the particle dynamics during bulk deformation could inspire the development of a nonequilibrium statistical theory that describes heterogeneous dynamics within bijels and their effect on the rheology.

Before closing, a note on the applicability of other functions to describe the nonlinear physics of interest in our model is warranted. Our choice of sigmoidal functions was based on the ability to fully tune the decay characteristics of each term using three adjustable parameters (shown in Fig. S4 in the supplementary material). The strain-induced softening and cage breaking dynamics modeled in our work can, in principle, be captured using other mathematical functions incorporated into the same basic double Maxwell framework. However, to simultaneously reproduce the Lissajous curve shapes and the softening characteristics observed in our frequency sweep experiments, we found that the use of functions whose decay characteristics could be fully tuned, such as a sigmoid, was necessary. For example, an alternative derivation of our model using hyperbolic functions with two adjustable parameters for each term captured some of the gross features of nonlinear bijel rheology with fewer adjustable parameters (see Figs. S5–S7 in the supplementary material) but was not able to reproduce the experimental results with the same fidelity as those presented in Figs 4 and 5 of this paper.

IV. CONCLUSIONS

The transition from linear-to-nonlinear rheology in bijels was investigated through experiments and qualitatively explained by a nonlinear double Maxwell model. Building upon our understanding of the continuous jammed interface in bijels, we developed a simple double Maxwell model whose relaxation time scales reflect Brownian-driven in-cage (β) and out-of-cage (α) dynamics, to explore the interplay between particle dynamics and interfacial deformation. Nonlinear oscillatory measurements revealed signatures of increased plasticity at high shear rates, which we attributed to local shear-induced local dilation and potential buckling of the interface along the extended and compressed regions of the interface, respectively. We incorporated nonlinear spring and dashpot elements into the double Maxwell model to account for the loss of viscoelasticity transpired by these events. Our model reproduces the linear frequency response of bijels observed in experiments and captures the general features of the linear-to-nonlinear transition including a backward-tilted stress response, the loss of elasticity at large strain amplitudes, the general shapes of Lissajous curves seen experimentally and frequency-dependent shear moduli that mimic the experimental data at medium strain amplitudes. Our findings suggest that bijel rheology is primarily dominated by the competition between α and β relaxation dynamics along the jammed interface, which are simultaneously interrupted and recovered by shear-induced stretching of the interface and recompaction by interfacial tension, respectively. Our model also suggests that some loss in the elastic modulus at intermediate strain amplitudes is likely related to events localized to high-rate portions of oscillation cycles such as buckling along the compressed regions of the interface. Our findings can form the basis for the development of more sophisticated models of bijel rheology based on shear-induced microstructural changes in the particle-laden interface. Some suggestions for future research on this topic include the use of more sophisticated statistical models to describe the particle dynamics along the interface; development of models that specifically take particle contact angles and their possible variations over time into account; extension of the model to systems in which particles form clusters or multilayers at the interface; the rheology of bijels that can form monogels; and accounting for possible changes in β relaxation dynamics (the $n = 1$ path in our system) upon shear-induced deformation.

SUPPLEMENTARY MATERIAL

See the supplementary material for a micrograph of the particles used in the study, experiments that monitor the formation and evolution of a bijel and the sample integrity during the lengthy frequency sweeps, plots of the sigmoid functions used in the study, and a test of hyperbolic tangent functions as an alternative to capture the nonlinear effects of interest.

ACKNOWLEDGMENTS

This research was funded by the NASA Research Opportunities in Complex Fluids and Macromolecular Biophysics Program (No. NNX13AQ69G). The authors thank the UCI Edwards Lifesciences Foundation Cardiovascular Innovation and Research Center for providing access to the Olympus Fluoview 3000 CLSM system (No. 1S10OD025064). The authors acknowledge the use of facilities and instrumentations (SEM and sputter coater) at the UC Irvine Materials Research Institute (IMRI), which is supported, in part, by the National Science Foundation through the UC Irvine Materials Research Science and Engineering Center (No. DMR-2011967).

AUTHOR DECLARATIONS

Conflict of Interest

The authors have no conflicts to disclose.

DATA AVAILABILITY

The data that support the findings of this study are available from the corresponding author upon reasonable request.

REFERENCES

[1] Stratford, K., R. Adhikari, I. Pagonabarraga, J. C. Desplat, and M. E. Cates, "Colloidal jamming at interfaces: A route to fluid-bicontinuous gels," Science **309**(5744), 2198–2201 (2005).

[2] Cates, M. E., and P. S. Clegg, "Bijels: A new class of soft materials," Soft Matter **4**, 2132–2138 (2008).

[3] Haase, M. F., K. J. Stebe, and D. Lee, "Continuous fabrication of hierarchical and asymmetric bijel microparticles, fibers, and membranes by solvent transfer-induced phase separation (STRIPS)," Adv. Mater. **27**(44), 7065–7071 (2015).

[4] Haase, M. F., H. Jeon, N. Hough, J. H. Kim, K. J. Stebe, and D. Lee, "Multifunctional nanocomposite hollow fiber membranes by solvent transfer induced phase separation," Nat. Commun. **8**(1), 1234 (2017).

[5] Günther, F., F. Janoschek, S. Frijters, and J. Harting, "Lattice Boltzmann simulations of anisotropic particles at liquid interfaces," Comput. Fluids **80**, 184–189 (2013).

[6] Cheng, H.-L., and S. S. Velankar, "Controlled jamming of particle-laden interfaces using a spinning drop tensiometer," Langmuir **25**(8), 4412–4420 (2009).

[7] Hijnen, N., D. Cai, and P. S. Clegg, "Bijels stabilized using rod-like particles," Soft Matter **11**(22), 4351–4355 (2015).

[8] Herzig, E. M., K. A. White, A. B. Schofield, W. C. K. Poon, and P. S. Clegg, "Bicontinuous emulsions stabilized solely by colloidal particles," Nat. Mater. **6**(12), 966–971 (2007).

[9] Witt, J., D. R. Mumm, and A. Mohraz, "Bijel reinforcement by droplet bridging: A route to bicontinuous materials with large domains," Soft Matter **9**(29), 6773–6780 (2013).

[10] French, D. J., A. B. Schofield, and J. H. J. Thijssen, "Bicontinuous soft solids with a gradient in channel size," Adv. Mater. Interfaces **9**(13), 2102307 (2022).

[11] Lee, M. N., and A. Mohraz, "Hierarchically porous silver monoliths from colloidal bicontinuous interfacially jammed emulsion gels," J. Am. Chem. Soc. **133**(18), 6945–6947 (2011).

[12] Lee, M. N., M. A. Santiago-Cordoba, C. E. Hamilton, N. K. Subbaiyan, J. G. Duque, and K. A. D. Obrey, "Developing monolithic nanoporous gold with hierarchical bicontinuity using colloidal bijels," J. Phys. Chem. Lett. **5**(5), 809–812 (2014).

[13] Witt, J. A., D. R. Mumm, and A. Mohraz, "Microstructural tunability of co-continuous bijel-derived electrodes to provide high energy and power densities," J. Mater. Chem. A **4**(3), 1000–1007 (2016).

[14] Cai, D., F. H. Richter, J. H. J. Thijssen, P. G. Bruce, and P. S. Clegg, "Direct transformation of bijels into bicontinuous composite electrolytes using a pre-mix containing lithium salt," Mater. Horiz. **5**(3), 499–505 (2018).

[15] McDevitt, K. M., D. R. Mumm, and A. Mohraz, "Improving cyclability of ZnO electrodes through microstructural design," ACS Appl. Energy Mater. **2**(11), 8107–8117 (2019).

[16] Santiago Cordoba, M. A., J. S. Spendelow, A. N. G. Parra-Vasquez, L. A. Kuettner, P. M. Welch, C. E. Hamilton, J. A. Oertel, J. G. Duque, E. J. Meierdierks, T. A. Semelsberger, J. C. Gordon, and M. N. Lee, "Aerobijels: Ultralight carbon monoliths from cocontinuous emulsions," Adv. Funct. Mater. **30**(6), 1908383 (2020).

[17] Gross, S. J., K. M. McDevitt, D. R. Mumm, and A. Mohraz, "Mitigating bubble traffic in gas-evolving electrodes via spinodally derived architectures," ACS Appl. Mater. Interfaces **13**(7), 8528–8537 (2021).

[18] Di Vitantonio, G., T. Wang, M. F. Haase, K. J. Stebe, and D. Lee, "Robust bijels for reactive separation via silica-reinforced nanoparticle layers," ACS Nano **13**(1), 26–31 (2019).

[19] Cha, S., H. G. Lim, M. F. Haase, K. J. Stebe, G. Y. Jung, and D. Lee, "Bicontinuous interfacially jammed emulsion gels (bijels) as media for enabling enzymatic reactive separation of a highly water insoluble substrate," Sci. Rep. **9**(1), 6363 (2019).

[20] Thorson, T. J., E. L. Botvinick, and A. Mohraz, "Composite bijel-templated hydrogels for cell delivery," ACS Biomater. Sci. Eng. **4**(2), 587–594 (2018).

[21] Thorson, T. J., R. E. Gurlin, E. L. Botvinick, and A. Mohraz, "Bijel-templated implantable biomaterials for enhancing tissue integration and vascularization," Acta Biomater. **94**, 173–182 (2019).

[22] Hsieh, M.-T., B. Endo, Y. Zhang, J. Bauer, and L. Valdevit, "The mechanical response of cellular materials with spinodal topologies," J. Mech. Phys. Solids **125**, 401–419 (2019).

[23] Zhang, Y., M.-T. Hsieh, and L. Valdevit, "Mechanical performance of 3D printed interpenetrating phase composites with spinodal topologies," Compos. Struct. **263**, 113693 (2021).

[24] Bonaccorso, F., S. Succi, M. Lauricella, A. Montessori, A. Tiribocchi, and K. H. Luo, "Shear dynamics of confined bijels," AIP Adv. **10**(9), 095304 (2020).

[25] Kharal, S. P., and M. F. Haase, "Centrifugal assembly of helical bijel fibers for pH responsive composite hydrogels," Small **18**(11), 2106826 (2022).

[26] Lee, M. N., and A. Mohraz, "Bicontinuous macroporous materials from bijel templates," Adv. Mater. **22**(43), 4836–4841 (2010).

[27] Lee, M. N., J. H. J. Thijssen, J. A. Witt, P. S. Clegg, and A. Mohraz, "Making a robust interfacial scaffold: Bijel rheology and its link to processability," Adv. Funct. Mater. **23**(4), 417–423 (2013).

[28] Macmillan, K. A., J. R. Royer, A. Morozov, Y. M. Joshi, M. Cloitre, and P. S. Clegg, "Rheological behavior and in situ confocal imaging of bijels made by mixing," Langmuir **35**(33), 10927–10936 (2019).

[29] Thijssen, J. H. J., and J. Vermant, "Interfacial rheology of model particles at liquid interfaces and its relation to (bicontinuous) Pickering emulsions," J. Phys.: Condens. Matter **30**, 023002 (2018).

[30] Ching, H., and A. Mohraz, "Bijel rheology reveals a 2D colloidal glass wrapped in 3D," Soft Matter **18**, 4227–4238 (2022).

[31] Cates, M. E., and P. S. Clegg, "Bijels: A new class of soft materials," Soft Matter **4**, 2132–2138 (2008).

[32] Mason, T. G., and D. A. Weitz, "Linear viscoelasticity of colloidal hard sphere suspensions near the glass transition," Phys. Rev. Lett. **75**(14), 2770–2773 (1995).

[33] Tavacoli, J. W., J. H. J. Thijssen, A. B. Schofield, and P. S. Clegg, "Novel, robust, and versatile bijels of nitromethane, ethanediol, and colloidal silica: Capsules, sub-ten-micrometer domains, and mechanical properties," Adv. Funct. Mater. **21**(11), 2020–2027 (2011).

[34] Rumble, K. A., J. H. J. Thijssen, A. B. Schofield, and P. S. Clegg, "Compressing a spinodal surface at fixed area: Bijels in a centrifuge," Soft Matter **12**(19), 4375–4383 (2016).

[35] Ewoldt, R. H., M. T. Johnston, and L. M. Caretta, Complex fluids in biological systems: Experiment, theory, and computation, in *Biological and Medical Physics, Biomedical Engineering* (Springer, New York, 2015).

[36] Bai, L., J. W. Fruehwirth, X. Cheng, and C. W. Macosko, "Dynamics and rheology of nonpolar bijels," Soft Matter **11**(26), 5282–5293 (2015).

[37] Pham, K. N., S. U. Egelhaaf, P. N. Pusey, and W. C. K. Poon, "Glasses in hard spheres with short-range attraction," Phys. Rev. E **69**(1), 011503 (2004).

[38] Petekidis, G., and N. J. Wagner, Rheology of colloidal glasses and gels, in *Theory and Applications of Colloidal Suspension Rheology*, 1st ed., edited by N. J. Wagner and J. Mewis (Cambridge University, Cambridge, 2021), pp. 173–226.

[39] Datta, S. S., D. D. Gerrard, T. S. Rhodes, T. G. Mason, and D. A. Weitz, "Rheology of attractive emulsions," Phys. Rev. E **84**(4), 041404 (2011).

[40] Sanatkaran, N., M. Zhou, and R. Foudazi, "Rheology of macro- and nano-emulsions in the presence of micellar depletion attraction," J. Rheol. **65**(3), 453–461 (2021).

[41] Kapnistos, M., A. N. Semenov, D. Vlassopoulos, and J. Roovers, "Viscoelastic response of hyperstar polymers in the linear regime," J. Chem. Phys. **111**(4), 1753–1759 (1999).

[42] Peters, B. L., K. M. Salerno, T. Ge, D. Perahia, and G. S. Grest, "Viscoelastic response of dispersed entangled polymer melts," Macromolecules **53**(19), 8400–8405 (2020).

[43] Parisi, D., E. Buenning, N. Kalafatakis, L. Gury, B. C. Benicewicz, M. Gauthier, M. Cloitre, M. Rubinstein, S. K. Kumar, and D. Vlassopoulos, "Universal polymeric-to-colloidal transition in melts of hairy nanoparticles," ACS Nano **15**(10), 16697–16708 (2021).

[44] Mendoza, A. J., E. Guzmán, F. Martínez-Pedrero, H. Ritacco, R. G. Rubio, F. Ortega, V. M. Starov, and R. Miller, "Particle laden fluid interfaces: Dynamics and interfacial rheology," Adv. Colloid Interface Sci. **206**, 303–319 (2014).

[45] de Souza Mendes, P. R., "Thixotropic elasto-viscoplastic model for structured fluids," Soft Matter **7**(6), 2471–2483 (2011).

[46] Kamani, K., G. J. Donley, and S. A. Rogers, "Unification of the rheological physics of yield stress fluids," Phys. Rev. Lett. **126**(21), 218002 (2021).

[47] Dimitriou, C. J., R. H. Ewoldt, and G. H. McKinley, "Describing and prescribing the constitutive response of yield stress fluids using large amplitude oscillatory shear stress (LAOStress)," J. Rheol. **57**(1), 27–70 (2013).

[48] Hyun, K., M. Wilhelm, C. O. Klein, K. S. Cho, J. G. Nam, K. H. Ahn, S. J. Lee, R. H. Ewoldt, and G. H. McKinley, "A review of nonlinear oscillatory shear tests: Analysis and application of large amplitude oscillatory shear (LAOS)," Prog. Polym. Sci. **36**(12), 1697–1753 (2011).

[49] Liu, A. J., and S. R. Nagel, "Jamming is not just cool any more," Nature **396**, 21–22 (1998).

[50] Janssen, L. M. C., "Mode-coupling theory of the glass transition: A primer," Front. Phys. **6**, 97 (2018).

[51] Ghosh, A., V. Chikkadi, P. Schall, and D. Bonn, "Connecting structural relaxation with the low frequency modes in a hard-sphere colloidal glass," Phys. Rev. Lett. **107**(18), 188303 (2011).